SOILS AND FOUNDATIONS Vol. 41, No. 3, 57–71, June 2001
Japanese Geotechnical Society

# FIELD AND LABORATORY MEASUREMENTS OF SMALL STRAIN STIFFNESS OF DECOMPOSED GRANITES

C. W. W. NG[i] and Y. WANG[ii]

## ABSTRACT

Non-linear stress-strain characteristics and stiffness-strain relationships of sedimentary soils and sands at small strains have been reported by many researchers. Research work on the behaviour of weathered or decomposed granites at small strains, however, has rarely been reported. This paper compares some stiffness measurements of decomposed granites from field investigations involving crosshole seismic, self-boring pressuremeter (SBPM), and high pressure dilatometer as well as results from laboratory tests using bender element and internal transducers. The in-situ crosshole measurements show that the elastic stiffness of Moderately Decomposed Granite (MDG, approximately 7000 MPa) is about 25% greater than that (about 5500 MPa) of Highly Decomposed Granite (HDG), which is in turn approximately 18 times higher than that (about 300 MPa) of Completely Decomposed Granite (CDG). This is likely attributable to the materials' different bond strengths and structures. A new method has been adopted to interpret the SBPM data. Measured data from crosshole seismic and self-boring pressure meter tests for CDG are found to be consistent. Bender element laboratory tests on CDG indicate that the measured A-coefficient in the expression of $G_0/p_r=A(p/p_r)^n$ lies between the results from clay and sand as reported in the literature. However, the measured n-value for CDG is generally larger for clays and sands. The measured bender element results are consistent with data from internal transducers. Highly non-linear characteristics of CDG were observed in both the laboratory and field tests. Generally the elastic stiffness of CDG as determined by laboratory tests is about 50–80% of that from field tests. Some possible reasons are discussed.

**Key words:** bonding and structure; decomposed granites; non-linear; shear and bulk modulus; stiffness (**IGC:** D6/D3)

## INTRODUCTION

Non-linear behaviour of most soils even at small strains ($0.001\% \leq \varepsilon_s \leq 1\%$) is widely accepted. Figure 1 shows an idealisation of soil stiffness for a wide range of strains. The shear modulus remains nearly constant at very small strains and decreases as the shear strain increases. At strains exceeding about 1%, stiffness is typically an order of magnitude less than the maximum, and it continues to decrease as failure approaches. The strain at which stiffness starts to decrease varies with plasticity from about 0.001% for low-plasticity soils to about 0.01% for plastic clays (Georgiannou et al., 1991). The non-linear stiffness-strain characteristics at small strains are very important for understanding deformations associated with soil-structure interaction problems. Typical soil strains mobilised near geotechnical structures such as retaining walls, foundations, and tunnels in stiff and hard soils such as stiff clays and dense sands generally fall within the classifications of small strain (Burland, 1989; Tatsuoka and Kohata, 1994). Much of the research and the numerical analyses related to non-linearity at small strains has been performed to study deformations in geotechnical engineering (Jardine et al., 1991; Tatsuoka and Shibuya, 1992; Simpson, 1992; Ng, 1992; Ng and Lings, 1995; Jiang et al., 1997; Ng et al., 1998a).

Hong Kong is a mountainous city subjected to prolonged subtropical climate conditions. Weathered granitic and volcanic rocks occupy most parts of Hong Kong. The geology of Hong Kong is briefly revealed in Fig. 2. Weathering generally can be classified into three types: chemical weathering (decomposition), physical weathering (disintegration), and biological weathering. In tropical and subtropical regions such as Hong Kong, chemical weathering is the dominant process. A six-fold rock material weathering grade classification scheme was recommended by the Geotechnical Control Office (GCO) in 1988 as reproduced in Table 1. This scheme is currently used in Hong Kong. It can be seen that the more intensively weathered the rock, the higher the weathering grade. Grade I (fresh granite), grade II (slightly decomposed granite) to grade III (moderately decomposed

[i] Associate Professor, Department of Civil Engineering, Hong Kong University of Science and Technology.
[ii] Research Student, ditto.

Manuscript was received for review on February 8, 2000.
Written discussions on this paper should be submitted before January 1, 2002 to the Japanese Geotechnical Society, Sugayama Bldg. 4F, Kanda Awaji-cho 2-23, Chiyoda-ku, Tokyo 101-0063, Japan. Upon request the closing date may be extended one month.

granite, "MDG") are generally considered as rock; whereas grade IV (highly decomposed granite, "HDG"), grade V (completely decomposed granite, "CDG") and grade VI (residual soil) are collectively known as soil. In geotechnical engineering terminology, MDG is a soft rock, and HDG and CDG are named as granitic saprolites, which still possess certain structure and bonding characteristics inherent in their parent rock (refer to Table 1).

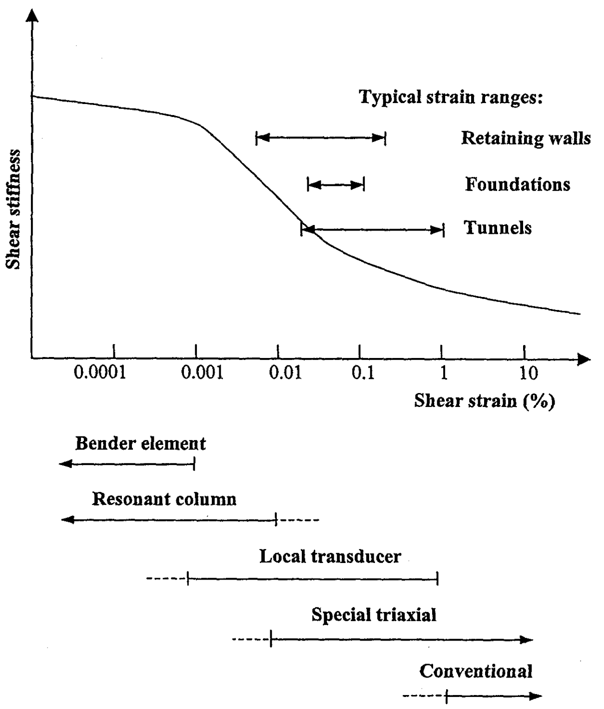


**Fig. 1. Approximate strain limits for soil structures in medium to dense or stiff soils (Mair, 1993)**

Many laboratory and field measurements of small strain stiffness have been conducted on sedimentary soils and soft rocks (Tatsuoka and Kohata, 1994; Viggiani and Atkinson, 1995; Jovicic and Coop, 1997; Tatsuoka et al., 1997). With a few exceptions such as Lee and Coop (1995), Viana da Fonseca et al. (1997) and Ng et al. (1998b; 2000), however, research on the stiffness-strain relationship of decomposed rocks and soils at small strains is relatively limited. Lee and Coop mainly focused on the study of the strength parameters of a recompacted decomposed granite from Korea, whereas Viana da Fonseca et al. concentrated their research on interpretation of the pressure-settlement curve from footing load tests in a granitic saprolite in Portugal. Ng et al. (1998b) published some stiffness measurements of a CDG from Kowloon Bay using local transducers only, but they did not have measurements of elastic modulus for useful comparisons. Ng et al. (2000) compared the laboratory measurements of CDG from Kowloon Bay with in-situ test results using self-boring pressuremeter and the suspension *P*-wave and *S*-wave logging method from the same site. However, the data were fairly scattered, especially at very small strains. As far as the authors are aware, no reliable test data and interpretations on small strain stiffness of MDG and HDG from Hong Kong has been reported in the literature.

In this research, the stiffness of decomposed granites including CDG, HDG and MDG was measured in-situ at Yen Chow Street for the new West Rail project by cross-hole seismic tests, self-boring pressuremeter and high pressure dilatometer tests, as well as in the laboratory by using bender elements and internal local transducers fit-

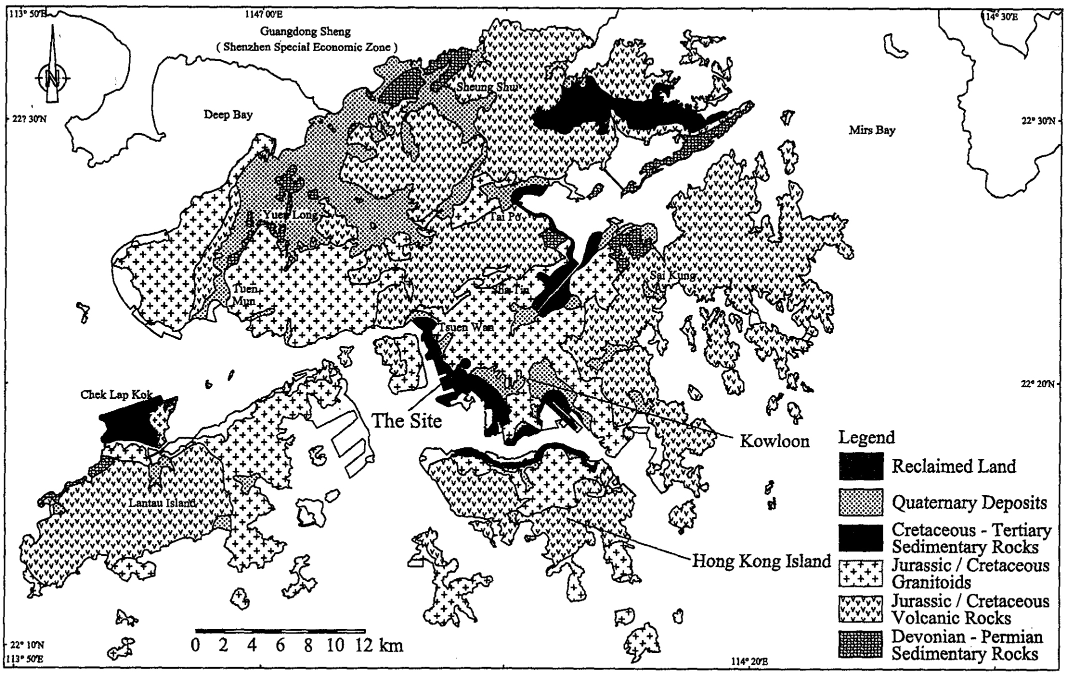


**Fig. 2. Geological map of Hong Kong showing location of test site**

**Table 1. Classification of granite decomposition grades of Hong Kong (from GCO, 1988)**

| Descriptive term | Fresh granite | Slightly decomposed granite | Moderately decomposed granite (MDG) | Highly decomposed granite (HDG) | Completely decomposed granite (CDG) | Residual soil |
|---|---|---|---|---|---|---|
| Grade symbol | I | II | III | IV | V | VI |
| Characteristics | Not broken easily by geological hammer<br>Makes a ringing sound when struck by geological hammer<br>No visible signs of decomposition (i.e. no discolouration)<br>Overall rock colour grey/white<br>Feldspars hard and shiny<br>Biotite shiny, not stained<br>Quartz colourless or grey, glassy | Not broken casily by geological hammer<br>Makes a ringing sound when struck by geological hammer<br>Fresh rock colours generally retained but stained near joint surfaces<br>Feldspars hard to slightly gritty<br>Orthoclase feldspars often pink<br>Biotite slightly stained and dull around edges<br>N Schmidt rebound value>45 | Cannot usually be broken by hand; easily broken by geological hammer<br>Makes a dull or slight ringing sound when struck by geological hammer<br>Completely stained throughout<br>Yellowish brown<br>Feldspars gritty<br>Biotite not shiny<br>N Schmidt rebound value 25–45 | Can be broken by hand into smaller pieces<br>Makes a dull sound when struck by geological hammer<br>Not easily indented by point of geological pick<br>Does not slake when immersed in water<br>Completely discoloured compared with fresh rock<br>Yellowish brown to yellowish orange/brown<br>Feldspars powdery<br>Hand penetrometer shear strength index >250 kPa<br>Positive N Schmidt rebound value<25 | Original rock texture preserved<br>Can be crumbled by hand and finger pressure into constituent grains<br>Easily indented by point of geological pick<br>Slakes when immersed in water<br>Completely discoloured compared with fresh rock<br>Yellowish brown to reddish brown<br>Feldspars powdery to soft<br>Hand penetrometer shear strength index <250 kPa<br>Zero rebound from N Schmidt hammer | Original rock texture completely destroyed<br>Can be crumbled by hand and finger pressure into constituent grains<br>Reddish brown<br>Feldspars completely destroyed<br>Quartz is only remaining primary mineral; usually dull, etched or pitted and reduced in size compared with fresh condition |

ted inside a triaxial apparatus. The objective of this research is to study comprehensively the behaviour of decomposed granites at small strains.

After obtaining high quality laboratory and field data and achieving a reasonable understanding of the small-strain characteristics of weathered granites, ideally appropriate constitutive model(s) specifically for the granites should be developed and applied in practice. In the meantime, high quality interpreted data can be adopted for back-analysing case histories using some existing strain and stress path dependent constitutive models such as the "Brick model" (Simpson, 1992). Once the selected model and model parameters have been calibrated with reliable and relevant case histories, they can be readily adopted for engineering design analysis in similar ground conditions. Alternatively, based on the back-analysis of mobilised shear strains in the ground, soil stiffness at the mobilised shear strain can be found and adopted in some simple models for engineering designs in similar ground conditions. Details of these approaches, and their advantages and disadvantages are explained by Ng et al. (1995). Moreover, the measured data can be used to assist engineers to estimate and modify their empirical design parameters.

## GROUND CONDITIONS AND SOME PHYSICAL PROPERTIES OF CDG

The study was carried out at one of the station sites of the new West Rail Project in Hong Kong. The test site is shown in Fig. 2 and the detail locations of boreholes are shown in Fig. 3. Two groups of boreholes, located about 300 m apart, were drilled to carry out ground investigation work and in-situ field tests. At the south of the site, three boreholes consisting of YCS1A, YCS1B and YCS1P were put down. Boreholes (YCS1A and YCS1B) were to provide access for in-situ crosshole seismic tests. High pressure dilatometer tests were conducted in bore-

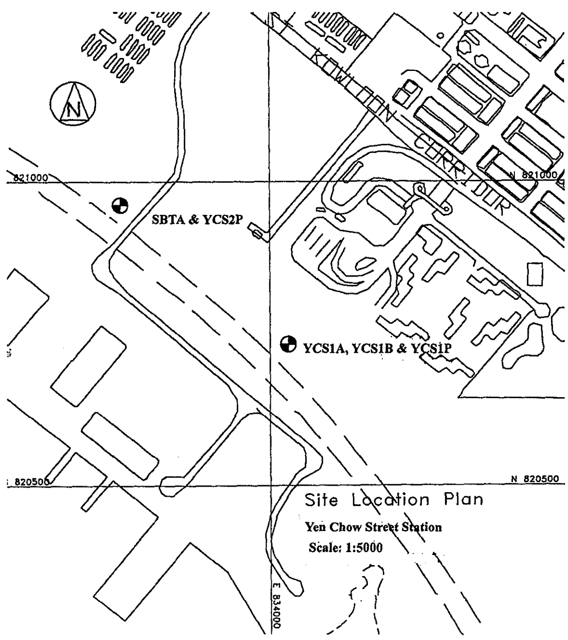


**Fig. 3. Locations of boreholes**

hole YCS1P. The distance between YCS1A and YCS1B is 6.12 m and borehole YCS1P is almost at the midpoint between them. In the northwest of the site, a second group of boreholes including YCS2P and SBTA was drilled. The distance between YCS2P and SBTA is 2.25 m. The former was put down to obtain high quality intact samples using a Mazier sampler (GCO, 1990) for laboratory testing and the latter was used for self-boring pressuremeter tests. The geology of the site comprises a sequence of fill and alluvium, overlying a thick layer of decomposed granites, which are medium to coarse grained. A simplified stratigraphy of the site is shown in Fig. 4. At the first group of boreholes (YCS1A, 1B and 1P), a linear variation of standard penetration $N$-value (SPT-$N$) with depth was consistently measured from the ground surface to about 43 m deep in the three boreholes. SPT-$N$ blow counts exceeding 200 were ignored at about 43 m deep or more. Three types of decomposed granites varying from Grade V (CDG) through Grade IV (HDG) to Grade III (MDG) were identified. At the second group of boreholes (YCS2P and SBTA), only a single layer of CDG, about 50 m thick, was found. The SPT-$N$ values in YCS2P varied almost linearly with depth to reach 200 at about 45 m below ground.

Some physical property measurements of CDG specimens taken from the site were conducted in the laborato-

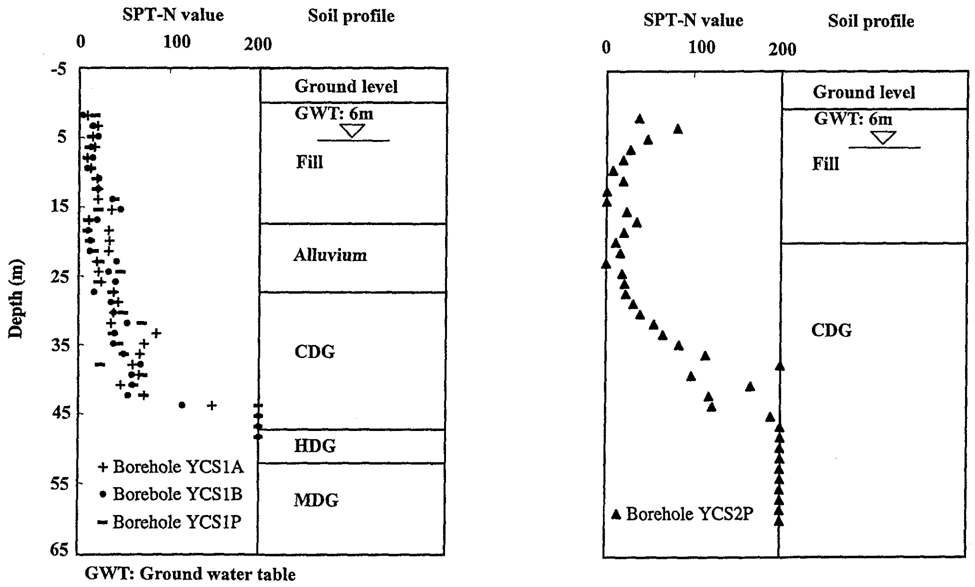


(a) Boreholes YCS1A, 1B, 1P

(b) Boreholes YCS2P, SBTA

**Fig. 4. Simplified stratigraphy of the site: (a) Boreholes YCS1A, 1B, 1P, (b) Boreholes YCS2P, SBTA**

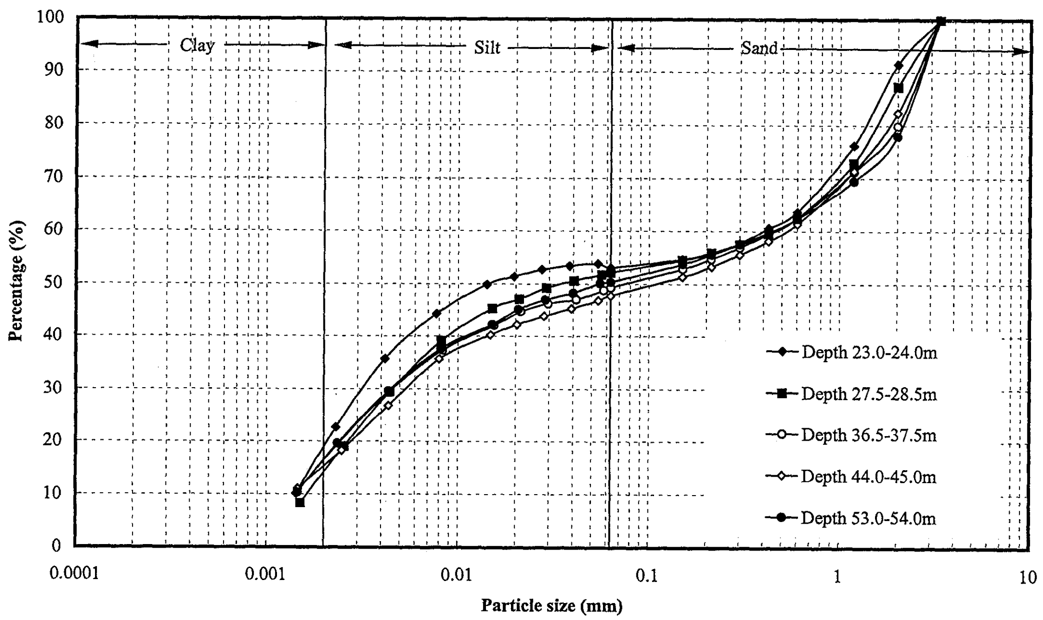


**Fig. 5. Particle size distributions of CDG**

ry. Figure 5 shows the particle size distributions of the specimens, which contain about 50% sand, 32% slit and 18% clay. The soil may be classified as clayey & sandy slit. The uniformity coefficient $C_u$ is estimated to be 250. Since the size of the soil particles (about 40%) is greater than 425 $\mu$m, this CDG is considered low plasticity soil, and no plasticity index can be determined.

## IN-SITU MEASUREMENTS OF SOIL AND WEAK ROCK STIFFNESS

### *Crosshole Seismic Measurements*

Geophysical methods are useful to access some material properties in ground investigations. Details of several geophysical methods are given by Dobrin (1988). Crosshole seismic tests measure seismic wave travel time and hence the in-situ shear wave velocity between two boreholes. Given that the in-situ bulk density of a material is known, the shear modulus of that material can be computed from travel time and path length.

In the crosshole seismic measurements presented in this paper, the seismic source was provided by a shear wave hammer. Horizontally propagating, vertically polarized shear waves ($S_{hv}$) were detected by a borehole-pick three-component geophone. In the borehole pick, three orthogonal geophone units are housed. The borehole pick is a three-axis borehole geophone of minimum diameter 43 mm. An expandable rubber packer tube allows the geophone to be coupled with the borehole walls for making the detection of shear waves possible. The signal from the geophone was recorded on a seismograph. The frequency of the shear waves was about 200 Hz. The distance between boreholes YCS1A and YCS1B at the surface was 6.12 m. The deduced path length of shear wave propagation at different depths along the boreholes varies from 6.07 m to 6.18 m. This shows that the verticality of boreholes is reasonably good. The shear wave velocity ($V_{hv}$) profile is presented in Fig. 6.

The shear wave velocity of CDG increases gradually from 29 m to 42 m. There is a gap at 43 m, and velocity increases quickly after that. This may be caused by a change of soil stratigraphy indicated by the measured SPT-*N* values. There is a noticeable change in the rate of increase of the SPT-*N* value with depth from 29 m to 42 m and from 43 m to 47 m (refer to Fig. 4a). According to the substantial increase in SPT-*N* values between 43 m and 47 m deep, a corresponding increase in measured stiffness at depths of 43 m to 47 m is expected. Moreover, the gap can be attributed to the "head" wave effect (Dobrin, 1988), caused by the arrival of a refracted "head" wave travelling in a stronger underlying stratum at the receiver before the direct wave travelling in the weaker overlying stratum. The velocity is likely to be overestimated at a depth just above the interface between the two strata and a correction is needed. A trend line along the velocities of CDG at depths far from the interface, which has less effect of "head" wave behaviour, is extended to the depth just above the interface to correct the "head" wave behaviour. The trend line between

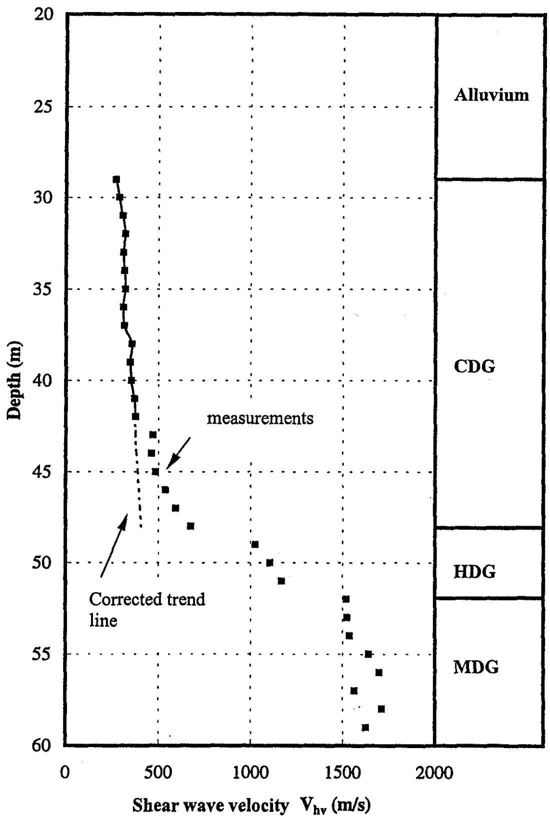


**Fig. 6. Shear wave velocity profile at boreholes YCS1A and YCS1B**

velocities and depth at depths 29 m to 42 m (the solid line in Fig. 6) is extended to the depth of 47 m (the dashed line in Fig. 6) to correct for the "head" wave effect. Given that the bulk densities of the materials are taken to be 2000 kg/m$^3$ at depths 29 m to 43 m, 2200 kg/m$^3$ at depths 44 m to 47 m, 2400 kg/m$^3$ at depths 48 m to 53 m, and 2550 kg/m$^3$ at depths 54 m to 59 m (as shown in Fig. 7), the variations of shear modulus $G_{hv}$ with depth can be calculated and are presented in Fig. 8. The $G_{hv}$ values at depths 43 m to 47 m were calculated with corrected shear wave velocities for the "head" wave behaviour (the dashed line in Fig. 6). The $G_{hv}$ values increase at a small rate initially from about 50 MPa corresponding to a depth of 29 m to about 250 MPa at 48 m within the CDG stratum (*see* Fig. 8). Between a depth of 48 m and 52 m, there is a significant increase in the shear wave velocity in the HDG layer (refer to Fig. 6). However, it is believed that the measured increase in shear wave velocity could have been affected by the "head" wave behaviour to some extent and could not be reliably accounted for properly due to the thin thickness of the HDG layer. Therefore, the measured data with this HDG zone are shown in Fig. 8 without any corrections and the interpreted stiffness of HDG is likely overestimated.

From the top for MDG, the values of $G_{hv}$ increase gently from about 5,500 MPa at a depth of 52 m to about approximately 7,000 MPa at a depth of 58 m but decrease slightly towards the depth of 60 m. The measured elastic stiffness of MDG is about 25% greater than that of

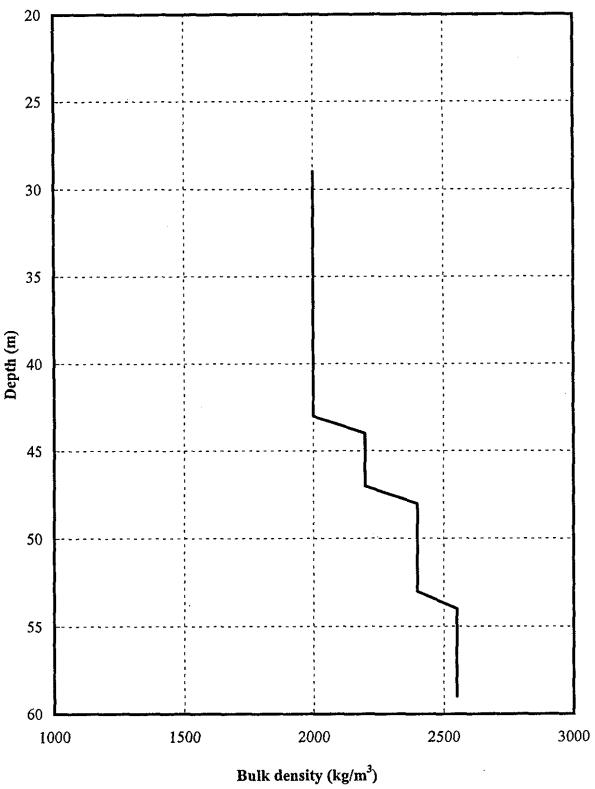


**Fig. 7. Relationship between bulk density and depth**

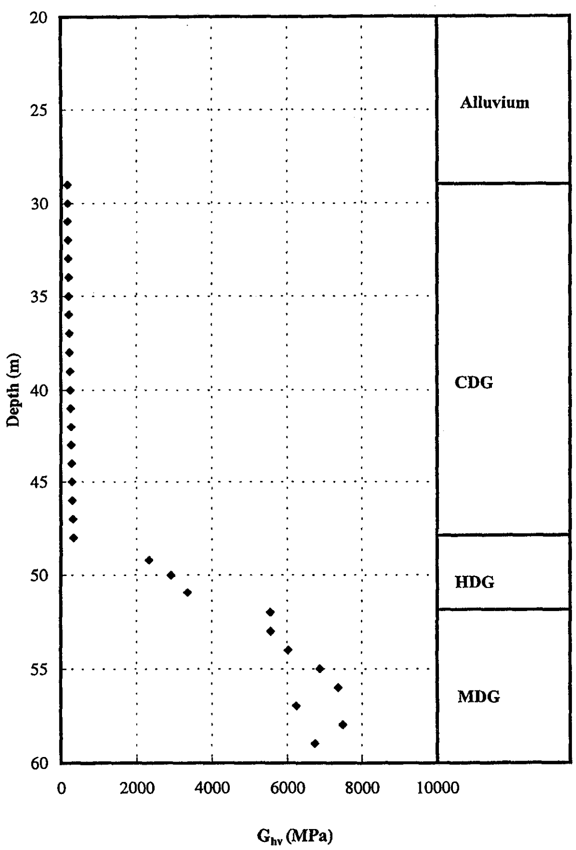


**Fig. 8. Variation of $G_{hv}$ with depth**

HDG, which is in turn approximately 18 times higher than that (about 300 MPa) of CDG at the bottom of each stratum. This is likely attributable to the materials' different bond strengths and structures. MDG is a soft rock and possesses a strong bonding and structure. In contrast, CDG only has weak bonding and structure.

The $G_{hv}$ profile is in agreement with the stratigraphy of boreholes YCS1A and YCS1B, which show a thick layer of CDG over the depths between 29 m and 47 m and HDG and MDG beginning at a depth of around 48 m and 52 m respectively.

### *Self-Boring Pressuremeter Measurements*

The purpose of a self-boring device is to enable a measurement device to be installed at a test location with minimum disturbance to soil. This enables the self-boring pressuremeter to perform a loading test on virtually undisturbed soil to determine in-situ stresses, strengths and deformation moduli. Details of self-boring pressuremeter tests are given by Clarke (1995). In order to evaluate the stiffness-strain relationships of CDG, four self-boring pressuremeter tests were carried out in borehole SBTA at depths of between 39.4 m and 48.5 m. A Cambridge self-boring pressuremeter was used. Calibration of the strain arms and pressure cells were conducted before and after the site work. Membrane stiffness and compressibility were measured before commencing testing and during the fieldwork for correction.

The borehole was put down by a drilling rig, and the self-boring of the pressuremeter was carried out with water flush using rotation and thrust from the drilling rig to achieve penetration of between 1.1 and 3.0 m. Following a relaxation period, typically 30 minutes, pressure was applied under computer control in a strain-controlled manner. Up to four unload-reload loops were carried out during each test with a holding period prior to each loop to minimize creep during the loop. The following relationship was adopted to avoid the ground failure in extension during the stress reversal from compression to extension: (Clarke, 1995)

$$\Delta p_c' \leq (p_c - u_0)_{max} \frac{2 \sin \phi'}{1 + 2 \sin \phi'}$$

where $\Delta p_c'$ is the range of unload and reload, $p_c$ is the cavity pressure, $(p_c - u_0)_{max}$ is the effective cavity pressure at the start of unloading, $u_0$ is the measured ambient pore pressure; and $\phi'$ is the estimated effective friction angle of the material.

### *New Method to Interpret Non-Linear Stiffness from Pressuremeter Tests*

Although the non-linear stress-strain characteristics of soils are well-recognised, there is still some difficulty in interpreting data from the pressuremeter tests. According to Muir-Wood (1990), the tangent to the cavity pressure-cavity strain relationship is equivalent to the secant modulus ($G_{sec}$) of soils. For the calculation of a tangent modulus, however, differentiation of in-situ measured data is needed. Due to unavoidable errors in the measurement

**Table 2. Summary of self-boring pressuremeter tests in CDG**

| Test no. | Depth (m) | $G_i$ (MPa) | $G_{ur}$ (MPa) | Cavity strain $\varepsilon_c$ (%) | New method (last loop only) | |
|---|---|---|---|---|---|---|
| | | | | | $G$ (MPa) | Shear strain $\varepsilon_s$ (%) |
| 1 | 39.4 | 54 | 234(1st loop)<br>218(2nd loop)<br>254(3rd loop)<br>206(4th loop) | 0.04(1st loop)<br>0.07(2nd loop)<br>0.06(3rd loop)<br>0.11(4th loop) | 250<br>221<br>202<br>178 | 0.02<br>0.06<br>0.08<br>0.11 |
| 2 | 42.4 | 47 | 204(1st loop)<br>213(2nd loop)<br>174(3rd loop) | 0.07(1st loop)<br>0.07(2nd loop)<br>0.13(3rd loop) | 258<br>222<br>163 | 0.03<br>0.06<br>0.12 |
| 3 | 45.0 | 44 | 219(1st loop)<br>335(2nd loop)<br>266(3rd loop) | 0.04(1st loop)<br>0.03(2nd loop)<br>0.08(3rd loop) | 279<br>255<br>220 | 0.03<br>0.06<br>0.09 |
| 4 | 48.5 | 63 | 301(1st loop)<br>269(2nd loop)<br>304(3rd loop) | 0.05(1st loop)<br>0.09(2nd loop)<br>0.07(3rd loop) | 313<br>276<br>236 | 0.03<br>0.06<br>0.09 |

systems, test data will not necessarily lie on a smooth curve, and simply differentiating the data will amplify these errors. There are two methods available to tackle this problem. Muir-Wood (1990) and Jardine (1991) suggest an empirical relationship to fit the experiment data and conduct differentiation on the fitted mathematical curve. Alternatively, Ferreira (1992), Robertson and Ferreira (1993), and Fahey and Carter (1993), and Fahey (1998) have developed another type of curve fitting method that incorporates a stress-strain constitutive model. The greatest weakness of the former method is that curve-fitting is just a numerical technique and it does not give any insight into the discrepancy between the measured data and the fitted curve. Thus, the fitted curve may not truly represent the test data. The weakness of the second method is that any improper predetermined soil model incorporated during data interpretation may impose unnecessary constraints and mask the true behaviour of soils.

In order to avoid the problems discussed above, a different approach (Li et al., 1998), which utilises a digital signal processing technique and applies it in geotechnical engineering, was adopted in this study. This digital signal processing method reduces the influence of high frequency noise during interpretations and eliminates any constraint of a pre-determined constitutive model on interpreted results. The key aspect of the digital signal processing technique is based on the sampling theorem and utilizes a noise-filtered differentiator to simultaneously differentiate the measured data and filter out the noise. The method performs true differentiation without an assumed mathematical expression. Details of the digital signal processing technique and applications are given by Li et al. (1998) and (Wang, 2000).

For interpreting measured data from self-boring pressuremeter tests, the secant modulus of soils was calculated with the following equation (Clarke, 1995):

$$G_{sec}=0.5(1+\varepsilon_{curr})\frac{dp_c}{d\varepsilon_{curr}}$$

where $G_{sec}$ is the secant modulus of soils or tangent modulus of pressuremeter tests, and $\varepsilon_{curr}$ is the current cavity strain which can be calculated as followed:

$$\varepsilon_{curr}=\frac{\varepsilon_c-\varepsilon_{um}}{1+\varepsilon_{um}}$$

Here $\varepsilon_{um}$ is the maximum cavity strain for the unloading portion, and $\varepsilon_c$ is the cavity strain.

*Results of Self-Boring Pressuremeter Tests*

All four sets of test data interpreted for all cycles using the traditional interpretation method (Clarke, 1995) are tabulated in Table 2. As expected, the shear modulus interpreted from the initial loading stage is substantially lower than those of the subsequently unloading/reloading loops. This is mainly because disturbance during installation of the pressuremeter may have induced substantial plastic strains in the surrounding soil. In order to ensure that the soil responds elastically, it is more satisfactory to determine the shear modulus of the soil from the slope of an unloading/reloading (Mair and Wood, 1987).

For interpreting the test data using the digital signal processing technique (Li et al., 1998), it was reasonable to ignore data from the first loading loop for the reason given in the previous paragraph. Moreover, since the measured data points from each subsequent unloading/reloading loop of the tests were very limited and hence the strain range was too small (i.e., 0.03–0.11%), they were not suitable for the digital signal processing method. Therefore, only the test results from the last complete unloading loop of each test were taken to evaluate the stiffness-strain relationship, and the interpreted results are also given in Table 2 for comparisons. At each strain level, the secant modulus of pressuremeter ($G_{ur}$) from each unload/reload loop agrees with the interpretation results using the digital signal processing technique. The non-linear characteristics of CDG interpreted using the digital signal processing technique are shown in Fig. 9. The secant modulus decreases significantly as shear strain increases. All four tests have similar non-linear

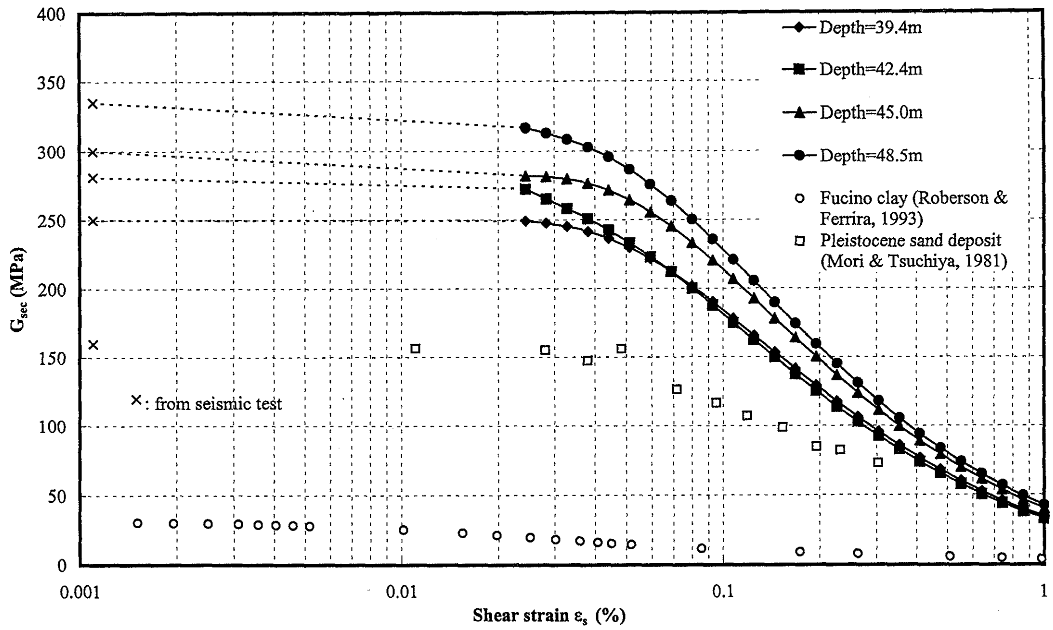


**Fig. 9. Non-linear characteristics from self-boring pressuremeter tests**

characteristics, and the magnitude of shear modulus increases as depth increases. As the shear strain increases, the test curves converge. The interpreted results from the crosshole seismic tests are also included in Fig. 9. They are fairly consistent with the pressuremeter tests and form the so called "S-shaped" shear stiffness-strain relationship. In Fig. 9, the results for Fucino clay (Robertson and Ferrira, 1993) and Pleistocene sand deposit (Mori and Tsuchiya, 1981) from pressuremeter and seismic tests are also included. They all show similar non-linear characteristics. However, the magnitude is quite different. The stiffness of CDG is about twice as large as that of Pleistocene and about ten times larger than that of Fucino clay at the same strain level. The strain thresholds of CDG and Pleistocene sand deposit are about 0.03%.

*High Pressure Dilatometer Tests*

A Cambridge high pressure dilatometer (Clarke, 1995) was used to perform two tests on loading the walls of borehole YCS1P to evaluate deformation and stiffness characteristics of HDG and MDG. The tests were carried out at depths of 51.5 m and 52.8 m. Calibration of the strain arms and pressure cells was carried out before and after the site work. Measurements of the membrane stiffness and compressibility were made before commencing testing and during the fieldwork for correction. Some of the interpreted test results are shown in Table 3. Generally the test results from the high pressure dilatometer are about twice to six times smaller than those obtained from the cross-hole seismic test results for MDG and HDG respectively. The difference may be caused by possible underestimation of stiffness due to disturbance using the dilatometer and possible overestimation of stiffness due to "head" wave effects during a seismic test, especially in the HDG layer. Nevertheless, the unload-reload shear modulus ($G_{ur}$) of MDG and HDG are larger than 3000 MPa and about 900 MPa, respectively, which are subsequently larger than that of CDG (about 300 MPa). The difference of modulus in decomposed granites is likely attributable to the difference in the materials' bonding strength and structure. MDG, HDG and CDG have the same parent rock but are subjected to different degrees of decomposition due to weathering (refer to Table 1), which leads to variations in bond strength and structure from strong to weak between the materials. MDG, which may be described as weak rock, is subjected to less weathering and has the strongest bonding and structure, and thus the largest shear modulus. CDG, which is a soil and may have weak bonding and structure, is decomposed completely. CDG's shear modulus is therefore the smallest.

**Table 3. Comparison between dilatometer and cross-hole seismic tests**

| Test no. | Depth (m) | Material type | $G_i$ from dilatometer (MPa) | $G_{ur}$ from dilatometer (MPa) | $G_{hv}$ from cross-hole (MPa) |
|---|---|---|---|---|---|
| 1 | 51.5 | HDG | 400 | 900 | 5500 |
| 2 | 52.8 | MDG | — | >3000<br>>3000<br>>3000 | 7000 |

## LABORATORY MEASUREMENTS OF STIFFNESS-STRAIN RELATIONSHIPS OF CDG

*Measuring Devices*

The laboratory tests were carried out using a computer-controlled stress path triaxial apparatus. Stiffness at small strains was measured using three Hall Effect internal transducers, including a pair of axial gauges and a single radial gauge. The resolution of the Hall Effect transducers is claimed to be 0.002% strain and the accuracy of the transducers can be as good as 0.01% strain (Clayton and Khatrush, 1986). The elastic shear modulus ($G_{\mathrm{vhlab}}$) at very small strains was obtained by using bender elements (Dyvik and Madshus, 1985; Viggiani and Atkinson, 1995). The modulus is determined by measuring the velocity of a shear wave travelling through the sample, which is similar in principle to the crosshole seismic tests. Arulnathan et al. (1998) pointed out that the delay time obtained from characteristic points or cross-correlation between the transmitted and received waves in bender elements tests is theoretically incorrect in most cases because: (1) the output signal of the receiving bender is measuring a complex interaction of incident and reflected waves; (2) the transfer functions relating the physical wave forms to the measured electrical signals introduce significant phase or time lags that are different at the transmitting and receiving benders; and (3) non one-dimensional travelling waves and near field effects are not accounted for. The errors due to the significant phase or time lags introduced by the instrumentation systems can be minimised to an acceptable level by using a powerful analyser. The transmitting bender can be regarded as a "point source" only for the ratio $\lambda/l_b$ is much larger than 4, where $\lambda$ is the wavelength of the signal and $l_b$ is the length of the bender element inserted into the soil specimen. On the other hand, the ratio $L/\lambda$ should be kept as large as possible in order to minimise a near-field effect, where $L$ is the path length of shear wave propagation. The frequency of the input signal therefore has to be chosen to balance these conflicting factors. Several excitation frequencies were tried in order to determine the best frequency for CDG. Some typical time histories of the transmitting and receiving waves of bender elements are shown in Fig. 10. It can be seen that the near field effect may easily mask first arrival of a shear wave when the excitation frequency is low (Fig. 10(a)). When the excitation frequency is too high, the output signals are also complicated, due to the invalidity of "point source" assumption (*see* Fig. 10(c)). When the optimum frequency (6 kHz) is adopted, the output signals are clear, and hence, the first arrival of the shear wave is well-defined (Fig. 10(b)).

The error of the bender element tests is mainly associated with an inaccurate determination of the first arrival of a shear wave. When the optimum frequency is adopted, the first arrival of a shear wave can be well recognised and hence the travel time of the shear wave can be determined with high accuracy. The error of elastic shear modulus obtained from the bender element tests in this paper is estimated to be less than ±5%.

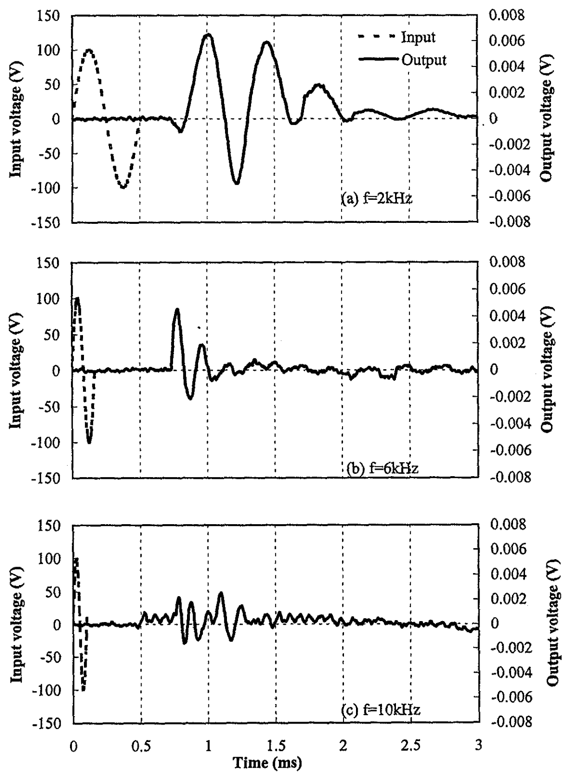


**Fig. 10. Effect of input signal frequency on output signal**

*Sample Preparation and Testing Procedures*

Laboratory tests were run with natural (intact) CDG specimens nominally 76 mm in diameter and 152 mm high, which were taken from borehole YCS2P using the Mazier sampling technique (GCO, 1990). Details of the test specimens are given in Table 4. After being extruded from a plastic PVC tube, the specimens were set into a 76 mm diameter plastic mould and both ends of the specimen were cut to a length of 152 mm with a wire saw. Great care was taken during the sample preparation to minimise disturbance. The samples were saturated with the de-aired water flowing from bottom to top under a high isotropic effective stress, which was estimated to be the mean effective stress in the field. This was to minimise any potential disturbance caused by a change of effective stress during saturation. Black and Lee (1973) relate the required Skempton's $B$ value for full or nearly full saturation to the soil stiffness. For stiff soils, a smaller $B$ value (less than 1) may be acceptable. Instead of using the traditional criterion for full saturation, a different saturation criterion suggested by Head (1986) was adopted. If several successive equal increments of confining (cell) pressure give an identical value of $B$, the specimens were considered as fully saturated, even though the $B$ value was less than 0.9 for stiff specimens (refer to Table 4). After saturation, three different series of tests were conducted to evaluate the stiffness of CDG at different strains: (1) a "B" series, determining elastic modulus using a bender element, (2) a "C" series, drained constant $p'$ compression tests, and (3) a "K" series, drained constant $q$ ($q=0$) test, with increasing isotropic confining pressure, where $p'$ and $q$ are the mean effective and deviator shear stress respectively. The first three numerical numbers in each sample identity denote the magnitude of initial mean

**Table 4. Details of intact CDG specimens**

| Sample identity | Depth (m) | $p_i'$ (kPa) | Test path or type | Initial moisture content before saturation (%) | Incremental $B$ value | $B$ value | Final moisture content (%) |
|---|---|---|---|---|---|---|---|
| 100B | 23.0–24.0 | 100 | Bender element test | 33.1 | 0.02 | 0.95 | 32.7 |
| 100C | 23.0–24.0 | 100 | Constant $p'$ compression test | 33.8 | 0.02 | 0.94 | 32.4 |
| 100K | 23.0–24.0 | 100 | Constant $q=0$ test | 33.3 | 0.02 | 0.94 | 32.1 |
| 150B | 27.5–28.5 | 150 | Bender element test | 28.5 | 0.03 | 0.94 | 27.0 |
| 150C | 27.5–28.5 | 150 | Constant $p'$ compression test | 27.4 | 0.05 | 0.89 | 27.3 |
| 150K | 27.5–28.5 | 150 | Constant $q=0$ test | 28.8 | 0.06 | 0.90 | 27.7 |
| 200B | 36.5–37.5 | 200 | Bender element test | 22.1 | 0.04 | 0.94 | 20.9 |
| 200C | 36.5–37.5 | 200 | Constant $p'$ compression test | 22.0 | 0.05 | 0.90 | 20.4 |
| 200K | 36.5–37.5 | 200 | Constant $q=0$ test | 21.0 | 0.05 | 0.88 | 19.8 |
| 250B | 44.0–45.0 | 250 | Bender element test | 19.1 | 0.04 | 0.86 | 18.0 |
| 250C | 44.0–45.0 | 250 | Constant $p'$ compression test | 17.1 | 0.04 | 0.84 | 16.9 |
| 250K | 44.0–45.0 | 250 | Constant $q=0$ test | 17.9 | 0.06 | 0.84 | 16.1 |
| 300B | 53.0–54.0 | 300 | Bender element test | 15.3 | 0.03 | 0.83 | 14.6 |
| 300C | 53.0–54.0 | 300 | Constant $p'$ compression test | 15.9 | 0.03 | 0.81 | 14.2 |
| 300K | 53.0–54.0 | 300 | Constant $q=0$ test | 15.0 | 0.03 | 0.84 | 13.5 |

Note: $p_i'$ is the estimated mean effective stress in the field.
Specific gravity $G_s$ of CDG: 2.64 $\mathrm{Mg/m^3}$

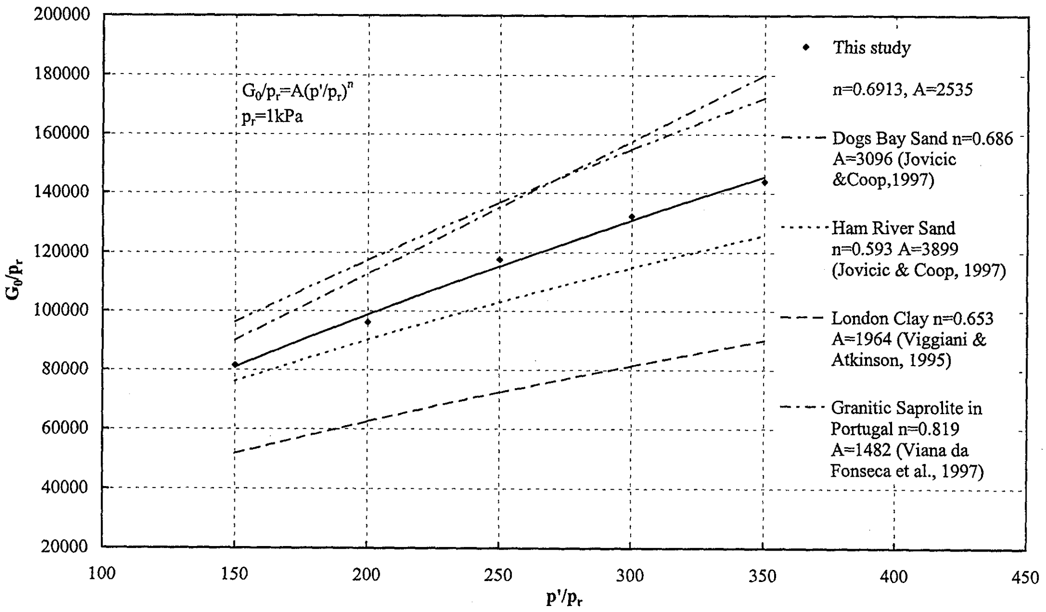


**Fig. 11. Normalised elastic shear modulus**

effective stress ($p_i'$). A slow test rate of 6 kPa to 7 kPa per hour was applied.

*Measurements of Elastic Shear Stiffness*

In order to measure $G_{vhlab}$ at different mean effective stresses ($p'$) using the bender elements, specimen 150B was isotropically consolidated from 150 kPa to 350 kPa. Shear wave velocity was measured, and, hence, $G_{vhlab}$ was determined at every 50-kPa interval. The measured $G_{vhlab}$ valves at every 50-kPa interval are shown in Fig. 11. Similar to sands and clays, an empirical power relationship between the $G_{vhlab}$ (or $G_0$) and $p'$ can be found for CDG and the relationship can be expressed as $G_0/p_r=A(p'/p_r)^n$, where $p_r$ is the reference pressure taken as 1 kPa. Based on $G_{vhlab}$ measurements, the values of $A$ and $n$ in the empirical power relationship were found to be 2535 and 0.691 respectively. Comparisons of the test results with the measured values of London Clay (Viggiani and Atkinson, 1995) and sands (Jovicic and Coop, 1997) are shown in Table 5. It is found that the A value of CDG lies between those of London clay (i.e., 1964) and sands (i.e., 3096-3899). On the other hand, the measured $n$ value (0.691) for CDG is a little bit higher than the reported values for London clay (0.653) and sands (0.593–0.686).

**Table 5. Comparison of elastic shear modulus between different soils**

| Soil type | $A$ value | $n$ value | Reference |
|---|---|---|---|
| Dogs Bay Sand | 3096 | 0.686 | Jovicic and Coop, 1997 |
| Ham River Sand | 3899 | 0.593 | Jovicic and Coop, 1997 |
| London Clay | 1964 | 0.653 | Viggiani and Atkinson, 1995 |
| Granitic Saprolite in Portugal | 1482 | 0.819 | Viana da Fonseca et al., 1997 |
| This Study | 2535 | 0.691 | Ng and Wang, 2000 |

Note: $A$ and $n$ values of Granitic saprolite in Portugal were calculated from measured elastic Young's modulus and Poisson's ratio.

Viana da Fonseca et al. (1997) studied the elastic stiffness of a natural granitic saprolite (CDG) in Portugal. They measured the elastic Young's modulus (E) and Poisson's ratio ($\nu$) in triaxial tests with internal strain gauges. The converted elastic shear modulus of granitic saprolite in Portugal was also shown in Fig. 11. As expected, the elastic shear modulus increases as confining pressure increases. However, the granitic saprolite in Portugal seems to be stiffer than CDG in Hong Kong.

Bender element tests were also carried out on specimens 100B, 200B, 250B and 300B to measure. $G_{vhlab}$ at isotropic confining pressures 100, 200, 250, 300 kPa, respectively. The test results are summarised in Table 6. As the mean effective stress varies from 100 kPa to 300 kPa, the measured $G_{vhlab}$ increases from 80 MPa (100B) to 196 MPa (300B).

*Variations of Shear Stiffness with Shear Strain*

For determining shear stiffness-shear strain characteristics, drained tests were carried out using a constant $p'$ stress path. Tests 100C, 150C, 200C, 250C and 300C were the compression tests conducted at constant $p_i'=100$, 150, 200, 250 and 300 kPa, respectively, where $p_i'$ is estimated in-situ mean effective stress. Figure 12 shows the normalised secant shear stiffness ($G_{sec}/p'$) against shear strain on the semi-logarithmic scale. For all the tests, it is evident that the shear stiffness of soil is highly non-linear and that stiffness decreases significantly as shear strain increases.

**Table 6. Comparison between measured stiffness in field and laboratory**

| Sample identity | Depth (m) | $p'$ (kPa) | $G_{vhlab}$ (MPa) | $G_{hv}$ from crosshole test (MPa) | Difference (%) |
|---|---|---|---|---|---|
| 100B | 23.0–24.0 | 100 | 80 | 113 | 29 |
| 150B | 27.5–28.5 | 150 | 82 | 147 | 44 |
| 200B | 36.5–37.5 | 200 | 104 | 197 | 46 |
| 250B | 44.0–45.0 | 250 | 142 | 294 | 52 |
| 300B | 53.0–54.0 | 300 | 196 | 389 | 50 |

Note: $G_{hv}$ at depths of 23.0–24.0 m and 53.0–54.0 m are extrapolated from the crosshole test results. $G_{vhlab}$ are measurements from bender element tests.

The "C" series test results fall to the lower bound of the test results on CDG specimens taken from Kowloon Bay (Ng et al., 1998b). The CDG specimens of Kowloon Bay were all taken from about 36 m below ground (estimated $p_i'=200$ kPa) but the test results were scattered. This is likely attributable to a significant variation in initial moisture content (i.e., 19.19%–35.15%) in the specimens from Kowloon Bay. However, the initial moisture content of the test specimens presented in this paper decreases as depth increases (refer to Table 4). Loss of moisture content of the soil specimen from Kowloon Bay during sample storage is a likely reason for the higher

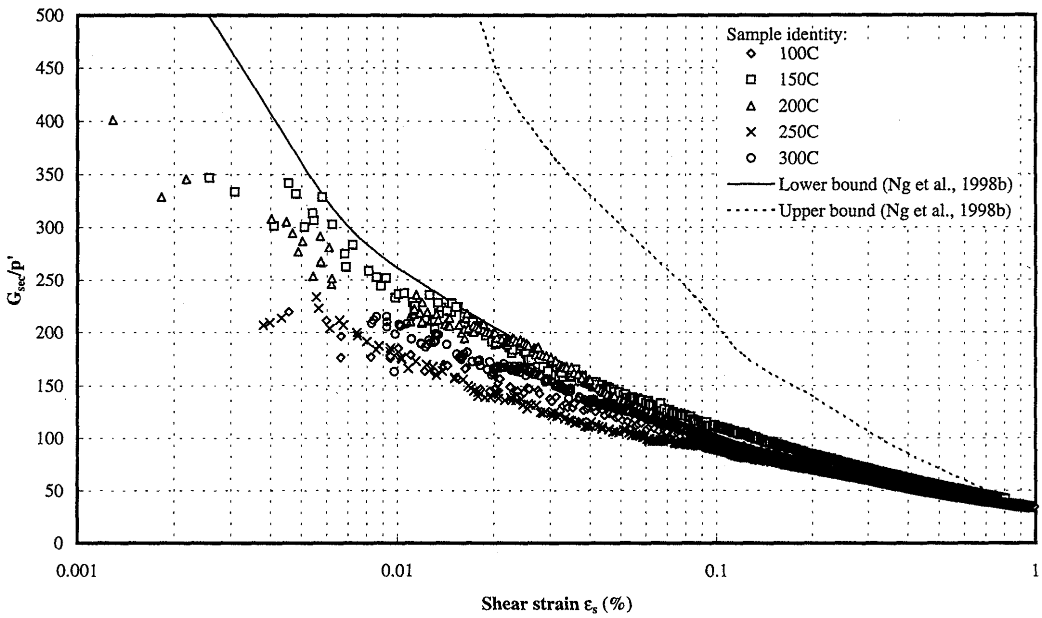


**Fig. 12. Variations of shear stiffness with shear strain of intact specimen**

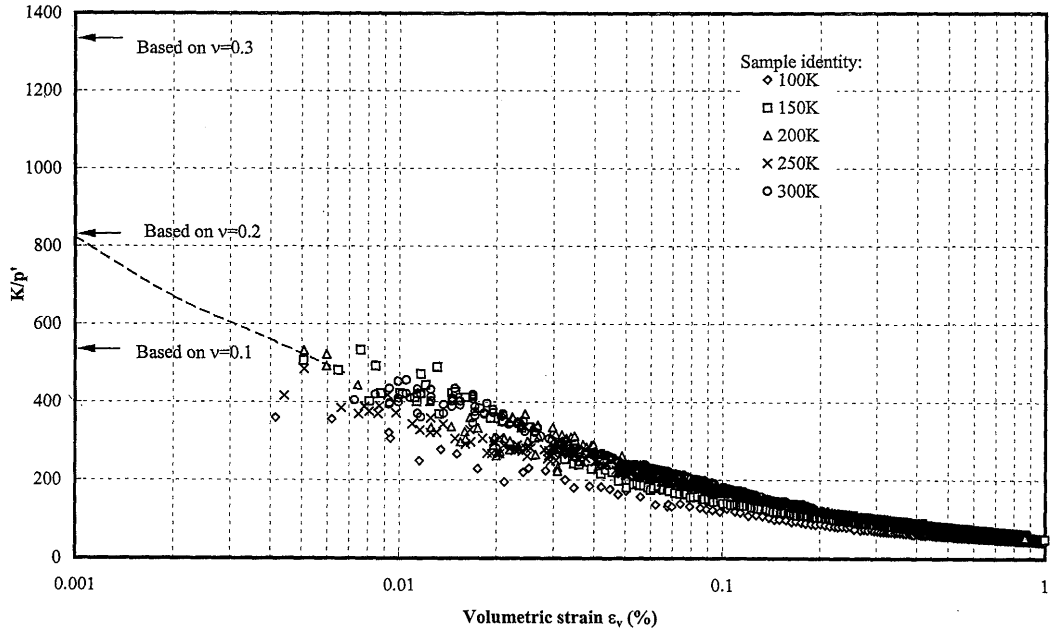


**Fig. 13. Variations of bulk modulus with volumetric strain of intact specimen**

stiffness. At 0.01% shear strain, the normalised shear stiffness is about 200, and the difference between the tests decreases as shear strain increases. At about 0.1%, the five sets of measurement appear to merge together with $G_{sec}/p'=100$. As the shear strain approaches 1%, the normalised shear stiffness of the CDG specimens drops below 50.

*Variations of Bulk Modulus with Volumetric Strain*

For evaluating the bulk modulus-volumetric strain characteristics, the soil specimens (100 K, 150 K, 200 K, 250 K and 300 K) were isotropically consolidated from initial mean effective stress ($p_i'$), which was estimated to be the mean effective stress in situ, to 400 kPa, respectively. Figure 13 shows the measured normalised secant bulk modulus ($K/p'$) versus volumetric strain on the semi-logarithmic scale. Perhaps, it is not surprising to see that the bulk modulus also decreases significantly as volumetric strain increases. $K/p'$ decreases from about 400 at 0.01% to about 50 at 1%. The maximum elastic bulk modulus ($K_{max}$) can be calculated by using elastic theory for isotropic material (i.e., $K_{max}=2G_0(1+\nu)/3(1-2\nu)$). By assuming a Poisson's ratio of 0.2, the $K_{max}$ value was calculated using the average value of the measured. The $K_{max}$ values calculated with $\nu=0.1$ and 0.3 are also shown in the figure. It is encouraging to see that the calculated $K_{max}$ value using $\nu=0.2$ matches quite well with the experimental data obtained by the Hall Effect transducers if a trend line is extrapolated (the dashed line in Fig. 13).

## COMPARISONS BETWEEN THE FIELD AND THE LABORATORY TEST RESULTS

*Elastic Shear Stiffness of CDG*

A comparison between $G_{hv}$ from crosshole seismic measurements in CDG and $G_{vhlab}$ obtained in the laboratory using bender elements is summarised in Table 6. Both sets of tests shows an increase in shear stiffness as depth or mean effective stress ($p'$) increases. The magnitude of $G_{vhlab}$ is, however, smaller than the magnitude of in-situ $G_{hv}$ ($G_{vhlab}=50$–80% $G_{hv}$). This may be attributable to differences in the field and laboratory stress conditions, and sample disturbance. In the laboratory, an isotropic mean effective stress, which was estimated from the ground condition by assuming $K_0$ value of 0.4 (Viana da Fonseca et al. 1997), was applied to CDG samples. However, it is obvious that the field stress condition is very different and is anisotropic in the ground. Stokoe et al. (1994) demonstrated that the travelling velocity of a shear wave is not only governed by stress in the direction of propagation but is also controlled to different extents by stress in the direction of polarisation. The isotropic stress state in bender element tests seems to underestimate the influence of stress on shear wave propagation in the vertical direction.

Although the Mazier sampling technique (GCO, 1990) was applied to obtain tube samples from the field and great care was taken during the sample transportation and sample preparation, some disturbance was inevitable. This is because natural CDG is generally believed to have some weak bonding, due to the inherent characteristics of the parent rock. The weak bonding is likely to be sensitive to disturbance. A soaking test was carried out to assess any bonding in the samples. The samples were soaked in the water and collapsed completely within a few minutes. It was clear that the samples' loss of bonding was either complete or they did not have any bond strength in the field.

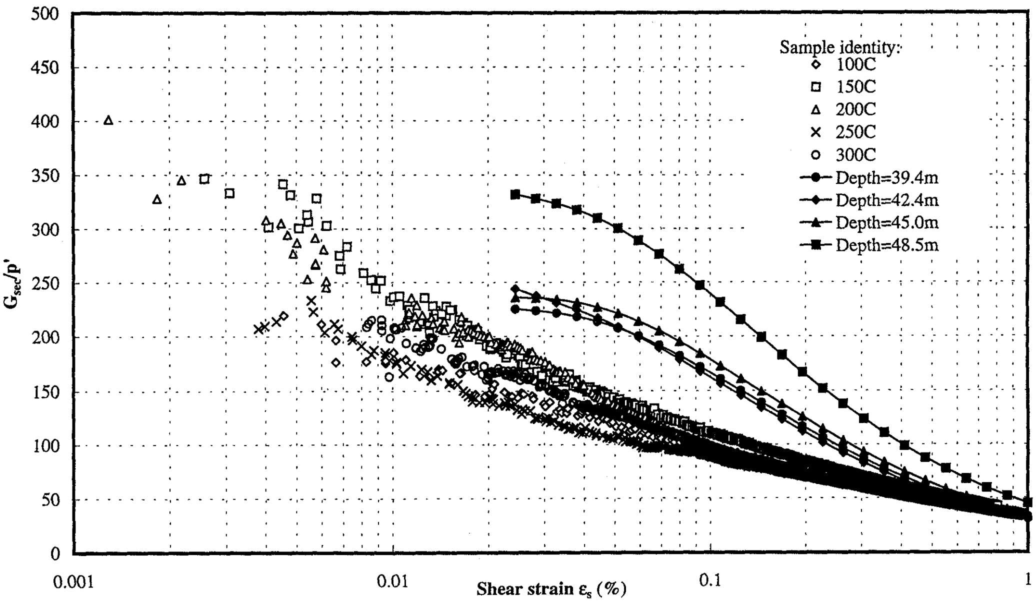


**Fig. 14. Comparisons between the field and laboratory tests**

*Non-Linear Characteristics of CDG*

For comparing the field and laboratory measured non-linear characteristics of CDG, Fig. 11 shows the measured modulus of the "C" series tests and the secant shear modulus from self-boring pressuremeter tests normalised to mean effective stress ($G_{sec}/p'$) versus shear strain on the semi-logarithmic scale. The mean effective stress used to normalise the pressuremeter test results is the average value of effective cavity expansion pressure ($\sigma_1'=p_c'$), effective overburden pressure ($\sigma_2'$), and the lateral earth pressure at rest ($\sigma_3'$). Because no reliable pore water pressure measurement is available, pore water pressure is taken as a hydrostatic state. For calculating $\sigma_3'$, a $K_0$ value has to be measured or estimated. It is extremely difficult to determine reliable horizontal stress and hence $K_0$ value from the self-boring pressuremeter tests in the completely decomposed granite or granitic saprolite from YCS2P, and so the measured $K_0$ value of 0.4 from a Portugal granitic saprolite (Viana da Fonseca et al., 1997) was applied to estimate $\sigma_3'$. It can be seen from Fig. 14 that both the field and the laboratory test results show significant non-linear characteristics. Shear modulus decreases as the shear strain increases. However, the $G_{sec}/p_0'$ from field tests is higher than that from laboratory tests. The $G_{sec}/p_0'$ value of the field tests varies from 230–330 to 50 as the shear strain increases from 0.02% to 1%. The $G_{sec}/p_0'$ value of the laboratory tests decreases from about 150 to 40 as the shear strain changes from 0.02% to 1%. The difference between them decreases and they tend to converge as the strain approaches 1%. It can also be seen that the strain thresholds in the laboratory test results and field test results are quite different. The strain threshold in the laboratory seems to be less than 0.001%, which is much smaller than that of the field tests (about 0.03%). The loss of bonding and structure resulting from sample disturbance is likely to be the main reason to explain the observed significant differences. During sampling, transportation, and preparation, intact samples are subjected to disturbances that cause loss of bonding and structure. Similar difficulties with Tokyo Bay clay (Tatsuoka et al., 1997), silica sandstone (Cuccovillo and Coop, 1997) and sand (Atkinson et al., 1990) have been reported in the literature. Cuccovillo and Coop concluded that existing bonding is the main factor that influences on the stiffness of structured sands. Atkinson et al. found that cemented sands have higher stiffness (about 4 times) and a larger strain threshold than those of uncemented sands.

The difference between the field test results and the laboratory test results shown in Fig. 14 can also be attributed to some other possible reasons such as different loading and boundary conditions and anisotropy of CDG. The loading conditions in the triaxial tests are axial symmetric, the sample is subjected to compression test, and boundary conditions are well-defined. The boundary and loading conditions of self-boring pressuremeter, on the other hand, are in fact very complicated (Atkinson and Sallfórs, 1991). The soil elements around the pressuremeter are subjected to different stresses, strains and stress paths (e.g. extension test mode). The modulus measured by this is simply an averaged soil property. Moreover, as far as the authors are aware, any anisotropic characteristics of the CDG have not been well-studied and published in the literature. If the stiffness of CDG is strongly anisotropic, then it may be another possible reason for the discrepancy observed between the laboratory and field test results.

## CONCLUSIONS

Both field and laboratory tests were carried out to study small strain stiffness characteristics of decomposed granites in Kowloon, Hong Kong. In the field, crosshole seismic tests, self-boring pressuremeter, and high pressure dilatometer tests were conducted. In the laboratory, bender elements and internal transducers (Hall Effect transducers) were adopted in a stress path triaxial apparatus. Based on the test results, several conclusions can be drawn:

1. The measured $G_{hv}$ profile from crosshole seismic tests between boreholes YCS1A and YCS1B is in agreement with the stratigraphy. The $G_{hv}$ value increases gradually at a small rate from a depth of 29 m to 47 m in completely decomposed granite (CDG). The $G_{hv}$ value increases rapidly from a depth of 48 m to 52 m in highly decomposed granite (HDG) and remains fairly constant below 53 m in moderately decomposed granite (MDG).
2. The in-situ crosshole measurements show that the elastic stiffness of MDG (7000 MPa) is about 25% greater than that (5500 MPa) of HDG, which is in turn approximately 18 times higher than that (300 MPa) of CDG at the bottom of each stratum. This is likely attributable to the materials' different bond strengths and structures. MDG is a soft rock and it possesses a strong bonding and structure inherited from its parent rock. In contrast, CDG may only have weak bonding and structure.
3. Elastic stiffness measurements of CDG using bender elements in the laboratory indicate that the measured A-coefficient in the expression of $G_0/p_r=A(p/p_r)^n$ lies between similar tests for clays and sands reported in the literature. However, the measured n-value for the CDG is larger than the measured n-value for London clay, Dog Bay and Ham River sands.
4. Comparing the field and laboratory measurements of elastic stiffness of CDG, the elastic stiffness as determined by the bender element tests is generally about 50–80% of that from the crosshole seismic tests. These discrepancies may be attributable to sample disturbance and different stress conditions in the field and in the laboratory.
5. Both self-boring pressuremeter tests in the field and laboratory triaxial tests show that the stiffness-strain characteristics of CDG are highly non-linear. The laboratory shear stiffness and bulk modulus decrease significantly as shear strain and volumetric strain increase, respectively. A markedly different method was adopted to interpret non-linearity of CDG from self-boring pressuremeter tests. The interpreted results from self-boring pressuremeter tests are consistent with the in-situ crosshole seismic tests and form a so called "S-shaped" non-linear stiffness-strain relationship. Similar non-linear stiffness-strain characteristics were also obtained in the laboratory using bender elements and internal local transducers. The self-boring pressuremeter test results indicate a greater stiffness and strain thresholds than those from the local transducers in the laboratory. At large strains, both field and laboratory-measured stiffnesses tend to converge.

## ACKNOWLEDGEMENTS

This research project is supported by a research grant CRC96/99.EG04 from the Co-operative Research Centre scheme and by a research grant RIG95/96.EG13 of the Research Grant Council of the Hong Kong Government of the Special Administrative Region (HKSAR). The authors would like to acknowledge the contributions provided by the Kowloon-Canton Railway Corporation (KCRC), Ove Arup and Partners Hong Kong Ltd. (OAP), all of whom provided some of the field test data analysed in this paper. In particular, the help of Messrs D. Gerken, I. Thomas, C. Calton, S. C. Lee and J. Blake of KCRC, Drs S. Hill, B. Littlechild and G. Plumbridge of OAP and Professors W. H. Tang and C. K. Shen of the HKUST are highly appreciated.

## NOTATION

$E$ = Elastic Young's modulus
$G_0$ = Elastic shear modulus
$G_{hv}$ = Elastic shear modulus obtained from horizontal propagating vertically polarised shear wave during crosshole seismic tests
$G_i$ = Initial shear modulus of pressuremeter tests
$G_{sec}$ = Secant modulus of soils
$G_{ur}$ = Secant modulus of pressuremeter tests
$G_{vhlab}$ = Elastic shear modulus from bender element tests using vertical propagating horizontally polarised shear wave
$K$ = Bulk modulus
$K_0$ = Coefficient of earth pressure at rest
$K_{max}$ = Maximum elastic bulk modulus
$L$ = Path length of shear wave propagation
$V_{hv}$ = Velocity of horizontal propagating vertically polarised shear wave in crosshole seismic tests
$k$ = Coefficient of permeability
$l_b$ = Length of bender element inserted into the soil specimen
$p_c$ = Cavity pressure in pressuremeter tests
$p_c'$ = Effective cavity pressure in pressuremeter tests
$p'$ = Mean effective stress
$p_0'$ = Mean effective stress in-situ measured from pressuremeter tests
$p_i'$ = Initial mean effective stress estimated in situ
$p_r$ = Reference pressure taking as 1 kPa
$q$ = Deviator shear stress
$u_0$ = Measured ambient pore pressure in pressuremeter tests
$\varepsilon_c$ = Cavity strain
$\varepsilon_{curr}$ = Current cavity strain
$\varepsilon_s$ = Triaxial shear strain
$\varepsilon_{um}$ = Maximum cavity strain for unloading portion
$\varepsilon_v$ = Volumetric strain
$\Phi'$ = Effective friction angle
$\lambda$ = Wavelength of the signal
$\nu$ = Poisson's ratio

## REFERENCES

1) Arulnathan, R., Boulanger, R. W. and Riemer, M. F. (1998): Analysis of bender element tests, *Geotechnical Testing Journal*, GTJODJ, **21** (2), 120–131.
2) Atkinson, J. H., Coop, M. R., Stallebrass, S. E. and Viggiani, G. (1990): Measurement of stiffness of soils and weak rocks in laboratory tests, *Proc. of 25th Annual Con. of Engrg. Geo. Group*, Leeds, British Geology Society, 21–27.
3) Atkinson, J. H. and Sallförs, G. (1991): Experimental determination of stress-strain-time characteristics in laboratory and in-situ tests, General report. *Proc. 10th Eur. Conf. Soil Mech. and Found. Engrg., Florence*, **3**, 915–956.

4) Black, D. K. and Lee, K. L. (1973): Saturating laboratory samples by back pressure, *J. Soil Mechanics and Foundation Division*, ASCE, **99**, SM1, paper 9484, 75-93.
5) Burland, J. B. (1989): Small is beautiful: the stiffness of soils at small strains, *Can. Geotech. J.*, **26**, 499-516.
6) Clarke, B. G. (1995): Pressuremeters in Geotechnical Design, Blackie Academic and Professional.
7) Clayton, C. R. I. and Khatrush, S. A. (1986): A new device for measuring local axial strains on triaxial specimens, *Géotechnique*, **36** (4), 593-597.
8) Cuccovillo, T. and Coop, M. R. (1997): Yielding and pre-failure deformation of structured sands, *Géotechnique*, **47** (3), 491-508.
9) Dobrin, M. D. (1988): Introduction to Geophysical Prospecting, 4th edn, McGraw-Hill, New York.
10) Dycik, R. and Madshus, C. (1985): Laboratory measurements of $G_{max}$ using bender elements, *Proc. Am. Soc. Civ. Engrs Conv.*, Detroit, 186-196.
11) Fahey, M. (1998): Deformation and in situ stress measurement, Geotechnical site characterization, *Proc. 1st Int. Conf. on Site Characterization*, Atlanta, Georgia, USA, 49-68.
12) Fahey, M. and Carter, J. P. (1993): A finite element study of the pressuremeter test in sand using a non-linear elastic plastic model, *Can. Geotech. J.*, **30**, 348-362.
13) Ferreira, R. S. (1992): Interpretation of pressuremeter tests using a curve fitting technique, *Ph.D. Thesis*, University of Alberta.
14) GCO (1990): Guide to site investigation Geoguide 2. Geotechnical Control Office (GCO), Civil Engineering Department, Hong Kong.
15) Georgiannou, V. N., Rampello, S. and Silvestri, F. (1991): Static and dynamic measurement of undrained stiffness of natural overconsolidated clays, *Proc. X ECSMFE, Florence*, **1**, 91-96.
16) Geotechnical Control Office (GCO), (1988): Guide to Rock and Soil Descriptions Geoguide 2. Geotechnical Control Office (GCO), Civil Engineering Department, Hong Kong.
17) Head, K. H. (1986): Manual of Soil Laboratory Testing. **3**, Pentech Press, London.
18) Jardine, R. J. (1991): Discussion on 'strain dependent moduli and pressuremeter tests,' *Géotechnique*, **41** (4), 621-626.
19) Jardine, R. J., Potts, D. M., St. John, H. D. and Hight, D. W. (1991): Some practical applications of a non-linear ground model, *Proc. X ECSMFE, Florence*, **1**, 223-228.
20) Jiang, G. L., Tatsuoka, F., Flora, A. and Koseki, J. (1997): Inherent and stress state-induced anisotropy in very small strain stiffness of a sand gravel, *Géotechnique*, **47** (3), 509-521.
21) Jovicic, V. and Coop, M. R. (1997): Stiffness of coarse-grained soils at small strains, *Géotechnique*, **47** (3), 545-561.
22) Lee, I. K. and Coop, M. R. (1995): The intrinsic behaviour of a decomposed granite soil, *Géotechnique*, **45** (1), 117-130.
23) Li, X. S., Yang, J. and Liu, H. L. (1998): Differentiation of noisy experimental data for interpretation of nonlinear stress-strain behavior, *Journal of Engineering Mechanics*, ASCE, **124** (7), 705-712.
24) Mair, R. J. and Wood, D. W. (1987): Pressuremeter testing—methods and interpretation, *CIRIA Ground Engineering Report: In-situ Testing*, Butterworths, London.
25) Mair, R. J. (1993): Developments in geotechnical engineering research: application to tunnels and deep excavations, *Proc. Inst. Civ. Engrs Civ. Engrg.*, **93**, Feb., 27-41.
26) Mori, H. and Tsuchiya, H. (1981): In-situ measurements on dynamic modulus and damping of Pleistocene soils, *Proc. Inst. Conf. On Recent Advances in Geotechnical Earthquake Engineering and Soil Dynamics*, St. Louis, **11**, 581-584.
27) Muir-Wood, D. (1990): Strain-dependent moduli and pressuremeter tests, *Géotechnique*, **40** (3), 509-512.
28) Ng, C. W. W. (1992): An evaluation of soil-structure interaction associated with deep excavations, *Ph.D. Thesis*, University of Bristol, U.K.
29) Ng, C. W. W. and Lings, M. L. (1995): Effects of modeling soil nonlinearity and wall installation on back-analysis of deep excavation in stiff clay, *Journal of Geotechnical Engineering*, ASCE, **121** (10), 687-695.
30) Ng, C. W. W., Simpson, B., Lings, M. L. and Nash, D. F. T. (1998a): Numerical analysis of a multipropped excavation in stiff clay, *Can. Geotech. J.*, **35**, 115-130.
31) Ng, C. W. W., Sun, Y. F. and Lee, K. M. (1998b): Laboratory measurements of small strain stiffness of granitic saprolites, *Geotechnical Engineering*, Southeast Asian Geotechnical Society, **29** (2), 233-248.
32) Ng, C. W. W., Pun, W. K. and Pang, R. P. L. (2000): Small strain stiffness of natural granitic saprolites in Hong Kong, *Journal of Geotechnical and Geo-environmental Engineering*, ASCE, **126** (9), 819-833.
33) Robertson, P. K. and Ferreira, R. S. (1993): Seismic and pressuremeter testing to determine soil modulus, Predictive soil mechanics, *Proc. Wroth Memorial Symp.*, Oxford, England, UK, 562-580.
34) Simpson, B. (1992): Retaining structures: displacement and design, *Géotechnique*, **42** (4), 541-576.
35) Stokoe II, K. H., Hwang, S. K. and Lee, J. N. K. (1994): Effect of various parameters on the stiffness and damping of soils at small strains. *Proc. Int. Symp. on Pre-failure Deformation Characteristics of Geomaterials, Hokkaido, Japan*, **2**, 785-816.
36) Tatsuoka, F. and Kohata, Y. (1994): Stiffness of hard soils and soft rocks in engineering applications, *Proc. Int. Symp. on Pre-failure Deformation Characteristics of Geomaterials, Hokkaido, Japan*, **2**, 947-1063.
37) Tatsuoka, F., Jardine, R. J., Lo Presti, D., Di Benedetto, H. and Kodaka, T. (1997): Characterising the pre-failure deformation properties of geomaterials, *Proc. 14th ICSMFE, Hamberg, Germany*, **4**, 2129-2164.
38) Tatsuoka, F. and Shibuya, S. (1991): Deformation characteristics of soils and rocks from field and laboratory tests, Keynote Lecture, *Proc. 9th ARCSMFE, Bangkok, Thailand*, **2**, 101-170.
39) Viana da Fonseca, A., Matos Fernandes, M. and Silva Cardoso, A (1997): Interpretation of a footing load test on a saprolitic soil from granite, *Géotechnique*, **47** (3), 633-651.
40) Viggiani, G. and Atkinson, J. H. (1995): Stiffness of fine-grained soil at very small strains, *Géotechnique*, **45** (2), 249-265.
41) Wang, Y. (2000): The characteristics of granitic saprolites at small strains, *M. Philos. Thesis*, Hong Kong University of Science and Technology, Hong Kong.